Microsystem Technologies
https://doi.org/10.1007/s00542-019-04409-z

TECHNICAL PAPER

Fabrication of hollow polymer microstructures using dielectric and capillary forces

Catherine E. H. Tonry[1] · Mayur K. Patel[1] · Weixing Yu[2] · Marc P. Y. Desmulliez[3] · Christopher Bailey[1]

Received: 14 March 2019 / Accepted: 18 March 2019

Abstract
Electric Field Assisted Capillarity is a novel one-step process suitable for the fabrication of hollow polymer microstructures. The process, demonstrated to work experimentally on a microscale using Polydimethylsiloxane (PDMS), makes use of both the electrohydrodynamics of polymers subject to an applied voltage and the capillary force on the polymers caused by a low contact angle on a heavily wetted surface. Results of two-dimensional numerical simulations of the process are discussed in this paper for the special case of production of microfluidic channels. The paper investigates the effects of altering key parameters including the contact angle with the top mask, the polymer thickness and air gap, the permittivity of the polymer, the applied voltage and geometrical variations on the final morphology of the microstructure. The results from these simulations demonstrate that the capillary force caused by the contact angle has the greatest effect on the final shape of the polymer microstructures.

1 Introduction

Electric field assisted capillarity (EFAC) is a novel process for fabricating enclosed and hollow polymer microstructures (Chen et al. 2012; Tonry et al. 2015). It is an extension of the electrohydrodynamic induced patterning (EHDIP), which is also known as LISA or lithographically induced self-assembly. With EHDIP, polymers above glass transition temperature can be manipulated to mimick the patterning on a top mask by use of electric fields (Wu and Chou 2005). This process stems from an instability in the surface of a polymer subject a uniform electric field generated, for example, by using a flat top electrode subject to an applied voltage. It was later shown that, if the spatial distribution of this electric field was configured by shaping the top electrode, the polymer would replicate this shape (Chou et al. 1999). The patterned polymer could then be hardened by thermal or UV-curing curing and keep the shape of the original electrode. The EFAC process, presented in Fig. 1, is an extension of EHDIP: the initial stage (labels *a* and *b* in the figure) is the same as in EHDIP. With EFAC the top electrode is also a heavily wetted surface which causes the polymer to be subject to a large capillary force, through the Lippmann effect, when it reaches the top mask (label *c*). This effect forces the polymer to coat the top electrode forming a shell of a few micrometers thick (label *d*).

The EFAC process is a single step encapsulation process that can be used to manufacture enclosed hollow microstructures, such as complex microchannels for microfluidic applications, waveguides for fiber optical communication systems and focusing lenses (e.g. LEDs) (Chen et al. 2012; Tonry et al. 2015). This article concentrates on the simulation of the formation of microchannels. There are two traditional methods for producing polymer microchannels. The first method, chemical etching, is based on processes used in micro fabrication in the microelectronics industry. It uses chemical reactions to remove a sacrificial layer forming a hollow microstructure (Peeni et al. 2006). This process relies on state-of-the-art control of the chemical reactions involved and deep understanding of microfluidics. Membrane-

✉ Catherine E. H. Tonry
C.Tonry@greenwich.ac.uk

[1] Computational Mechanics and Reliability Group (CMRG), Centre for Numerical Modelling and Process Analysis, University of Greenwich, 30 Park Row, London SE10 9LS, UK

[2] Xi'an Institute of Optics and Precision Mechanics, Chinese Academy of Sciences, Xi'an, Shaanxi, China

[3] Microsystems Engineering Centre (MISEC), School of Engineering and Physical Sciences, Heriot-Watt University, Earl Mountbatten Building, Edinburgh EH14 4AS, UK

Published online: 27 March 2019

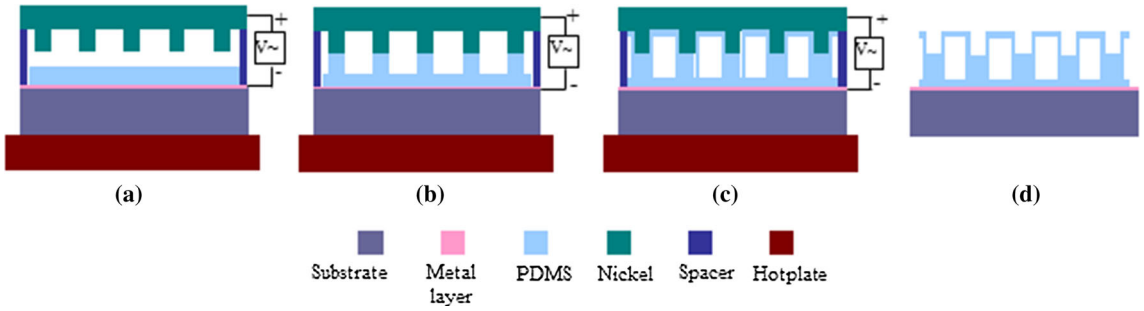

Fig. 1 Schematic of the EFAC process

assisted micro-transfer molding is the second method whereby a membrane is bonded to microchannels which have been molded using soft lithography (Unger et al. 2000). This process requires two stages: firstly molding the channels and secondly capping them with a thin membrane. The EFAC process has advantages over both of these methods, as it is an electromechanical process rather than a chemical one and it is also a single step process. It is likely therefore to be cheaper than both methods in use. Current experimental work has shown that this process works for a variety of shapes, even producing complex structures such as microchannels and capsules, as shown later on, as well as a combination of these structures (Unger et al. 2000). The relatively few studies carried out on this promising process put a large uncertainty over the length of time taken to manufacture hollow structures and more experimental research needs to be done; however, an initial upper limit of 1 h for shaping and curing has been demonstrated (Chen et al. 2012).

The model described in this paper was developed to further investigate the key operational parameters of the process and how it could be extended to industrial scale.

2 Description of the process

EFAC makes use of the electrohydrodynamic and surface tension properties of liquid polymers. Experiments on the process so far have all used the low surface tension PDMS polymer, though the process should work using other polymers of similar surface tension. The process is presented schematically in Fig. 1 and explained here in more details. The experiment set up consists with a top patterned electrode and a bottom electrode. A low surface tension liquid polymer (PDMS) is coated onto the bottom electrode. Optional spacers can be used to separate the two electrodes so that there is an air gap in between the top electrode and the polymer surface. A hotplate is used to heat the polymer above glass temperature for thermally curable polymers (a). The electric field is generated by applying a potential difference across the two electrodes which destabilizes the thin polymer film and induces the microstructure growth upward towards the top electrode. The shape of the mask causes the electric field to be higher at the interface under the lower parts of the mask, then due to the higher electric field in these regions the charge density at the surface is higher causing the electric force to be greater compared to the surface at the higher parts of the mask. This variation in force causes the molten polymer to flow up in the regions closest to the mask. The electric field becomes even larger in these regions accelerating the process (b). The fluid eventually reaches the top mask where the capillary force becomes dominant due to a very low contact angle from the heavily wetted top mask. With a low contact angle, this capillary force is sufficient to cause the material to flow completely around the mask (c). After the hollow microstructures are formed, the polymer is cured and then released from the top electrode. Although not represented in the schematic, the formed hollow microstructures present a curved lower surface due to the system reaching equilibrium between surface tension and air pressure. The process works also with UV-cured polymers. In that case a hotplate is not necessary and the solidification of the polymer is carried out using UV flood exposure of the polymer.

3 Numerical model

The numerical model used to simulate the process was built using the COMSOL^{TM} Multiphysics 4.3b software package using the electrostatics and laminar phase field modules. The laminar phase field module solves fluid flow and the position of the air/polymer interface while the electrostatics module resolves the electric field.

The laminar phase field module in COMSOL solves the Navier–Stokes equations combined with a diffuse interface phase field model to simulate the multiphase flow. Due to

the small length scales of microchannels and the high viscosities of polymers, the Reynolds number is assumed to be low and the flow laminar. The equations were solved using the finite element solver within COMSOL and the PARDISO direct solver, which is a parallel direct solver for sparse matrices.

The diffuse interface phase field model (Yue et al. 2004) in COMSOL describes the interface based on the mixing energy of the fluid. This is in contrast to level set models, which use an artificial smoothing function to describe the fluid at the interface. The adoption of this model has two key benefits: the curvature at the interface is obtained directly from the method simplifying surface tension calculations and viscoelastic flows can be directly included in the mixing energy. This method separates the Cahn–Hilliard equation into two coupled Helmholtz equations that are solved to describe the surface in terms of the free energy.

$$\frac{\partial \phi}{\partial t} + \boldsymbol{u} \cdot \nabla \phi = \nabla \frac{\lambda \gamma}{\epsilon_{pf}^2} \psi, \tag{1}$$

$$\psi = -\nabla \cdot \epsilon_{pf}^2 \nabla \phi + (\phi^2 - 1)\phi + \frac{\epsilon_{pf}^2}{\lambda} \frac{\partial f}{\partial t}, \tag{2}$$

where ϕ is the phase field variable, ψ the phase field helper variable, $\mathbf{u}$ the velocity, λ the length scale of a volume element, γ the surface tension coefficient, ϵ_{pf} the capillary width. Flow is solved using the laminar Navier–Stokes equations:

$$\rho \frac{\partial \mathbf{u}}{\partial t} + \rho(\mathbf{u} \cdot \nabla)\mathbf{u} - v\nabla^2 \mathbf{u} = \boldsymbol{f}. \tag{3}$$

The electric field is calculated by solving Poisson's equation for the voltage and the electric field is then calculated from the gradient of the voltage. The force $\boldsymbol{f}$ at the interface is a result of the dielectric forces (Landau and Lipshitz 1984).

$$\boldsymbol{f} = \frac{1}{2} \nabla \left[\boldsymbol{E}^2 \rho \left(\frac{\partial \varepsilon}{\partial \rho} \right)_T \right] - \frac{1}{2} \nabla \varepsilon, \tag{4}$$

where $\boldsymbol{f}$ is the force per unit area, $\boldsymbol{E}$ the electric field, $\boldsymbol{\rho}$ density and $\boldsymbol{\varepsilon}$ the permittivity.

The material properties, given in Table 1, are for PDMS and are based on those used in experiments (Chen et al. 2012). A separation distance of 10 mm has been chosen between the bottom of the top electrode and the top surface of the deposited polymer. Although the viscosity value of the polymer is already high, an increased viscosity has been used to damp the flow and ensure convergence; this is due to the large forces concentrated around the interface. The simulations presented here are for a top electrode with rounded corners for the grooves of the pattern as shown in Fig. 2, along with the boundary conditions. The mesh of Fig. 2a) represents a single channel and a symmetry plane has been included. Rather than using sharp-angled corners which can lead to singularities in the electric field equation the corners have been smoothed.

For simplicity it is also assumed that the air and polymer are both incompressible and the temperature is constant, as these would have little effect on the solutions. In addition, the viscoelastic nature of the liquid polymer has been neglected as we are only interested in the final shape of the polymer and an artificially high viscosity is already used.

4 Results

Figure 3 shows the simulated morphological change of the liquid polymer as it is electrostatically pulled towards the top electrode for a contact angle of 20° between the polymer and the surface of the top electrode. The force on the fluid is greater under the lower sections of the mask due to the increased electric field; this causes the polymer to flow upwards at these points (a). When it reaches the top mask (b) the surface tension causes the fluid to flow around the mask (c) finally reaching a steady state and coating the mask (d). This is the general evolution of the flow for complete cases. The final stage of the simulation is shown in Fig. 3d. Steady state is however reached at around 37 ms. Figure 4 demonstrates the evolution of the electric field over the same time period.

4.1 Influence of the contact angle

Figure 5 shows the influence of contact angles ranging from 10° to 25° on the resulting manufacture hollow microstructures. A lower contact angle causes a thicker shell to form. Figure 5c shows that, if the contact angle is too large, the capillary force becomes too small to fully encapsulate the hollow microstructures. There is a large variation in the thickness of the polymer, with the top of the cap and sides being thinner than the corner.

Table 1 Material properties of PDMS

Simulation dynamic viscosity (centipoise)	Specific gravity (25 °C)	Dielectric constant (100 Hz)	Surface tension (mN/m)
1000	1.03	2.72	20

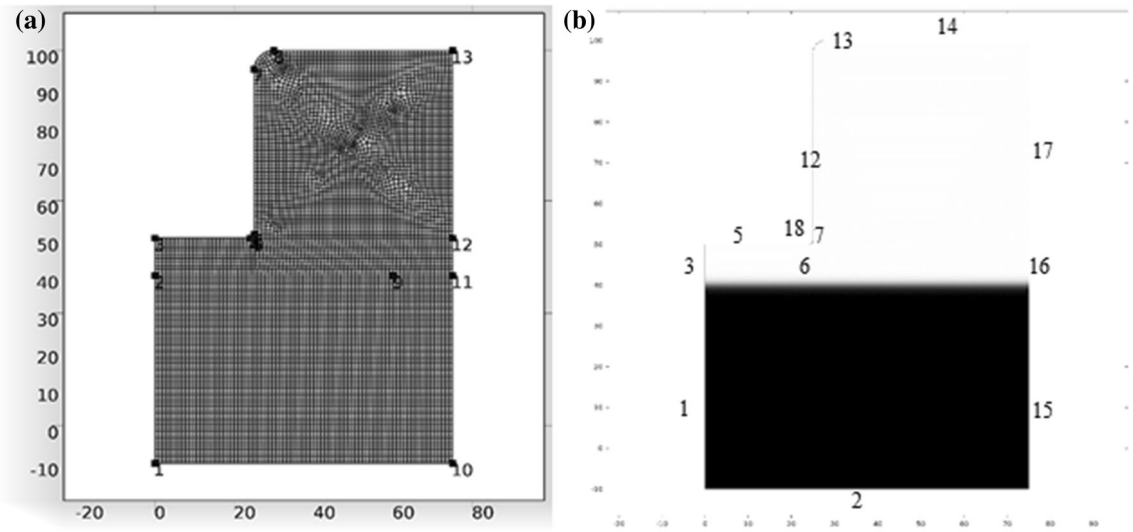

	Flow	Electric Field		Flow	Electric Field
1	Slip Wall	Symmetry	12	Wetted Wall	250 V
2	No-Slip Wall	0 V	13	Wetted Wall	250 V
3	Slip wall	Symmetry	15	Symmetry	Symmetry
5	Slip wall	250 V	16	Symmetry	Symmetry
6	Wetted Wall	N/A	17	Symmetry	Symmetry
7	Wetted Wall	N/A	18	N/A	250 V

Fig. 2 Mesh (**a**), geometry (**b**) and boundary conditions (**c**). Dimensions are in μm

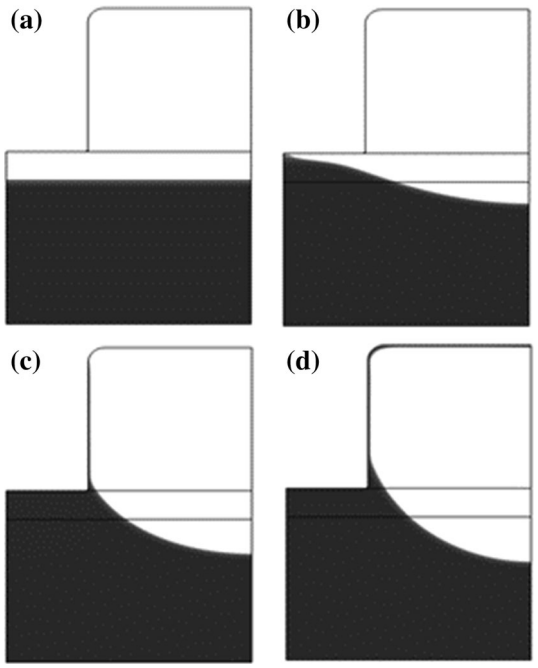

Fig. 3 Evolution of the polymer surface at **a** 0 s, **b** 27 ms, **c** 32 ms and **d** 100 ms

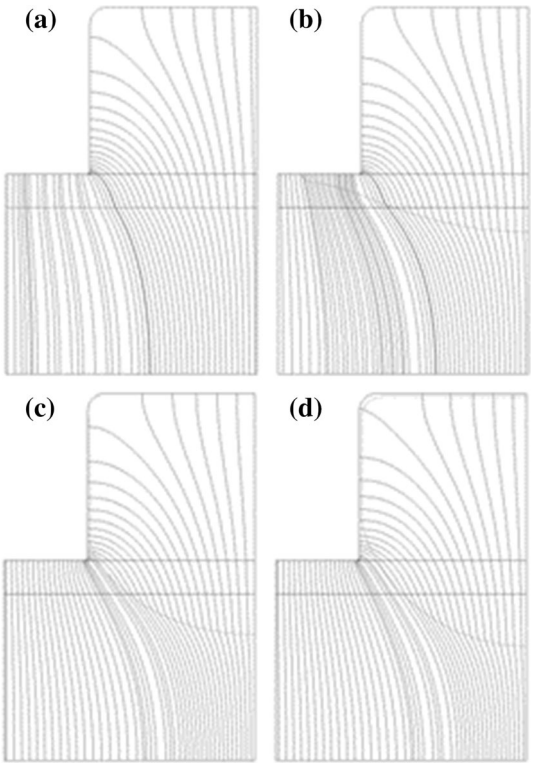

Fig. 4 Evolution of the electric field at **a** 0 s, **b** 27 ms, **c** 32 ms and **d** 100 ms

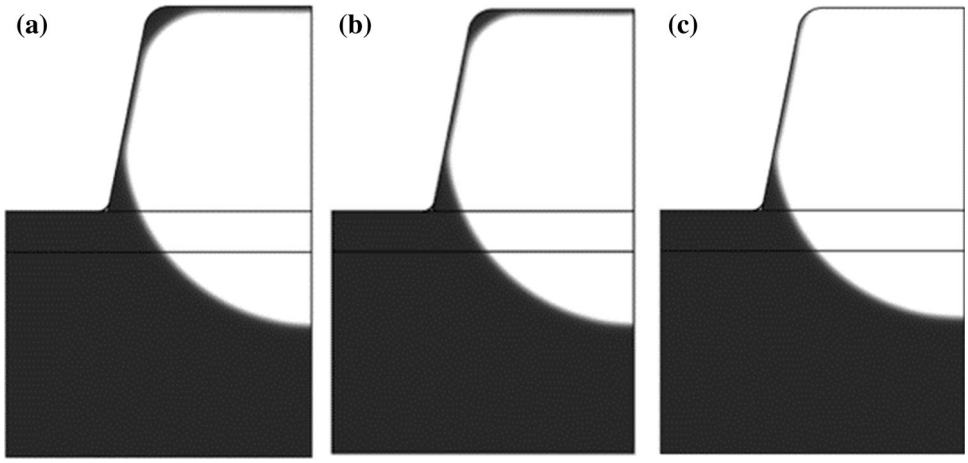

Fig. 5 Influence of the contact angles for the top electrode **a** 10°, **b** 20° and **c** 25°

4.2 Influence of the air gap and initial polymer thickness

Figure 6a is the result of the simulation of the resulting microchannel for an air gap of 50 µm instead of 10 µm. The larger air gap creates a deeper channel and an angular bottomed channel is formed instead of a rounded one as in the previous case. A layer of polymer remains on the bottom electrode as this is also a wetted surface. Figure 6b shows also the formation of a microchannel with a thicker initial polymer for an air gap of 10 µm. The same thin surface is kept on the surface of the top electrode but a much deeper channel is produced compared to the case of a thin initial polymer. Dimensions are shown here for both figures as the geometry is different to the original case.

4.3 Influence of the permittivity value of the polymer

The influence of the value of the permittivity of the polymer permittivity was also investigated as shown in Fig. 7. There cases were run, one with the polymer with a very low permittivity of $\in = 1$ (the same as air) and two other cases with relative permittivity values of 2.5 and 5. A permittivity of 1 is a useful verification case as no change in permittivity at the interface gives no dielectric force and so the polymer surface remains at its initial position. Indeed, Fig. 7a shows that the interface does not deviate from its initial condition.

Comparing the influence on the final shape of the microstructure of the choice of permittivity, as shown in Fig. 7b and c, highlights that the final shape is minimally dependent on the permittivity of the polymer. Figure 7d shows the influence of all the different permittivity values used, with the lines representing the surface of the polymer. These results demonstrate that changing the permittivity of

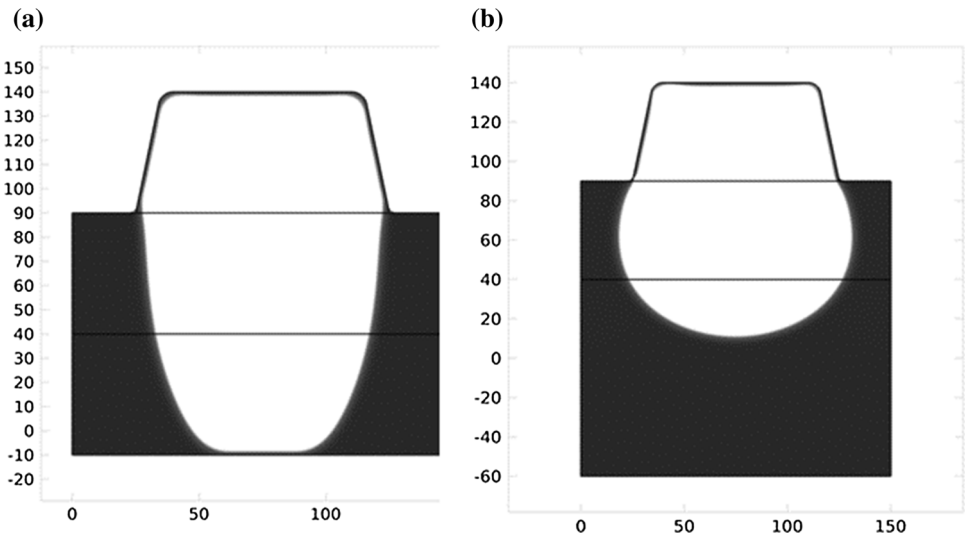

Fig. 6 Influence of the air gap (**a**) and polymer thickness (**b**) on the formation of the hollow microstructure. Dimensions are in µm

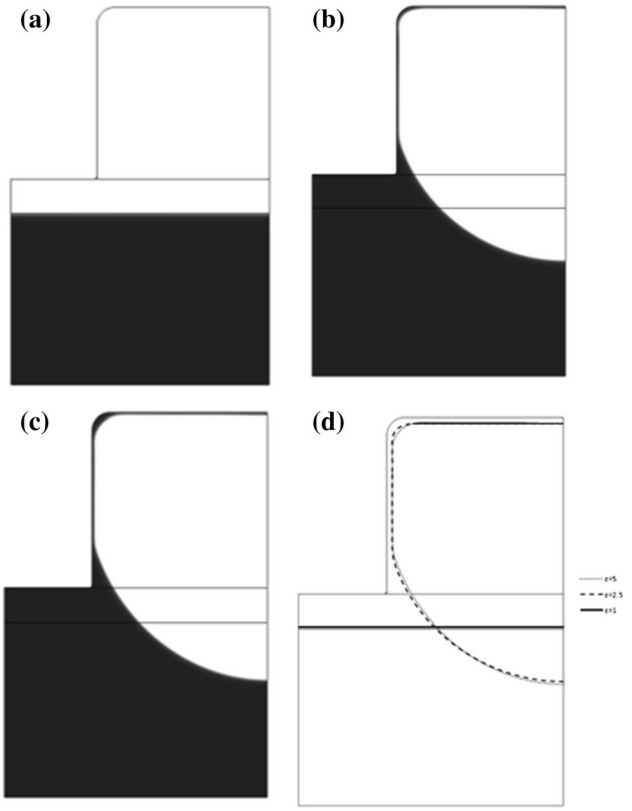

Fig. 7 Influence of the permittivity value of the polymer **a** ε = 1, **b** ε = 2.5, **c** ε = 5, **d** combined showing all 3 permittivity values

the polymer has a limited effect on the final shape. If the permittivity is too low there will not be enough force to overcome surface tension. With increasing permittivity values, the bubble inside the polymer changes shape, but only marginally. The speed of the initial stage is also increased with a higher dielectric due to a higher dielectric force.

4.4 Influence of the difference of potential

Figure 8 shows the influence of the voltage applied across the top electrode on the resulting microstructure with applied voltages of 100 V, 250 V, 500 V and 1000 V. Conditions for absence of electrical breakdown between the top electrode and the surface of the polymer were not verified. In the first case, shown in Fig. 8a, the dielectric forces at the interface are unable to overcome surface tension forces and so the surface of the polymer only exhibits a small deflection. The most apparent effect is the increasing speed of the process with increasing voltages where the polymer touches the bottom of the top electrode within 31 ms, 3.2 ms and 0.8 ms for voltages of 250 V, 500 V, and 1000 V, respectively. From an industry perspective the voltage is a key operating parameter to enable a high throughput process.

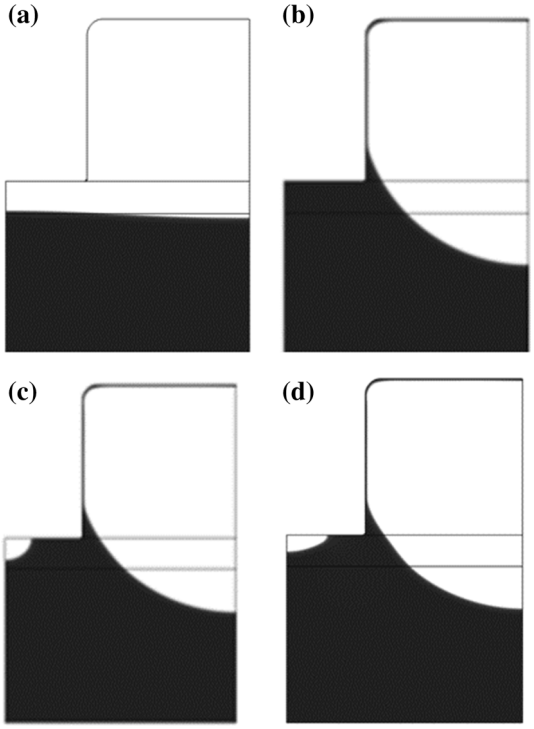

Fig. 8 Influence of change of potential: **a** 100 V, **b** 250 V, **c** 500 V and **d** 1000 V

Figure 8b–d also show that the final shape is altered in a similar fashion as the change of the permittivity values. This is to be expected from the dielectric force Eq. (4) as increasing the voltage increases the interfacial dielectric forces. Note also that, for the highest voltage case, a bubble remains in the left-hand corner of the mask. This represents a defect indicating an upper limit on the process speed for maximum process yield.

4.5 Influence of the pattern of the top electrode

Figure 9 shows the effect of small changes to the corner of the electrode shape. Three corners of radii of 2 μm, 3 μm and 5 μm were investigated. Although the variation between these cases is relatively small, the change in the local electric field is significant enough to alter the direction of the interfacial forces such that, for sharp corners, the top electrode is unable to create a fully enclosed structure.

5 Comparison with Experiments

Figure 10 presents a comparison of the model to an electron micrograph image taken of the capsules created experimentally. Further information on the experimental setup can be found in Chen et al. (2012). Such structures have the advantage to offer over a small area the

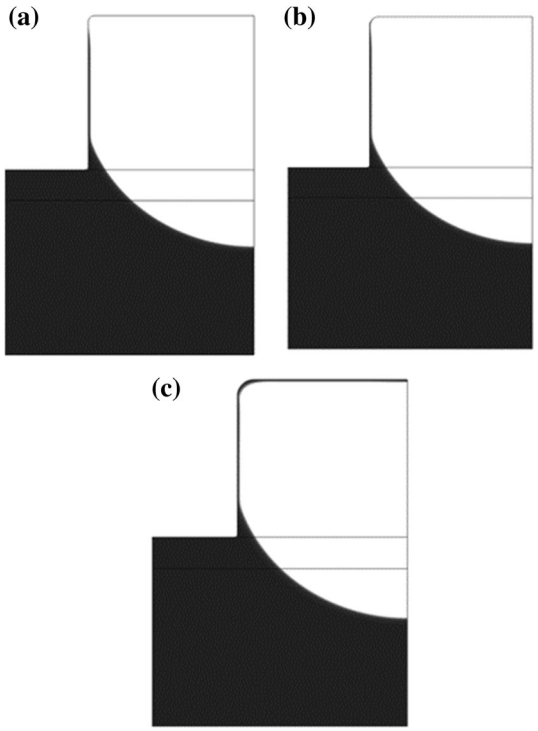

Fig. 9 Influence of the radius of the corner of the top electrode **a** radius = 2 μm, **b** radius = 3 μm and **c** radius = 5 μm

experimental validation of our modelling results. The square capsules are large enough (around 100 μm width) such that a long channel approximation should apply on a cross section through the center. The shell of the capsule on the left hand side of Fig. 3 shows tears at the top and at the side as highlighted by the dark circles. This loss of mechanical integrity is due to a narrowing of the cap on the numerical model for earlier time steps. Based on modelling results, the hole at the top of the capsule is likely due to insufficient material, whereas the side breakage seems to be a function of the mask shape. The cut apart capsules demonstrate a thicker surface compared to the model. However this is likely due to the increased surface tension force caused by the corners of the capsules, a fully 3D model would be required to fully investigate this phenomenon. No such thickening was seen for the long microchannel as shown in Fig. 11. These microstructures form a similar thin layer of only a few microns thickness as in the numerical model. The curved base of the channel as demonstrated in the model is also seen.

6 Conclusions

A numerical model has been developed using the Multiphysics simulation software package COMSOL™. The simulation model allowed the capture of the key features of the EFAC process, such as the fabrication speed, morphology of the fabricated part and failure modes that can result from poor process parameters and material properties. This multiphysics model incorporated dielectric forces coupled with free surface flow algorithms. The model allowed for the effects of key process parameters and material properties to be investigated in the EFAC process.

This paper explored the general behaviour of key process parameters including:

- Initial thickness of the deposited polymer,
- relative permittivity of the polymer,
- air gap between polymer and the top electrode,
- shape of the top electrode,
- contact angle of between the liquid polymer and the top electrode,
- voltage applied across the two electrodes.

Of these process parameters, this study suggests that poor contact angle and electrode shape are more likely to cause process failure (i.e. not forming enclosed structures). Fabrication speed can be controlled by the voltage. However, if it is too quick then bubbles can form in the

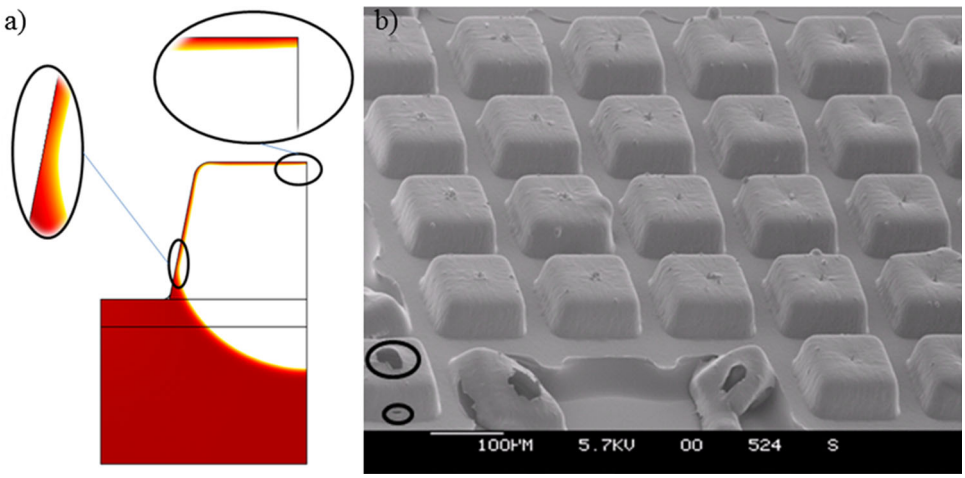

Fig. 10 Comparison of numerical model (left hand side figure) to experiments (right hand side figure). Black circles on both figures highlight the regions of minimum

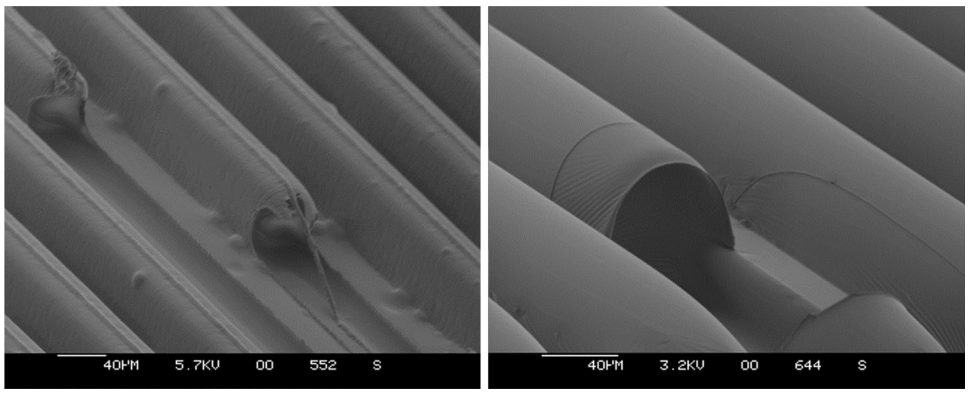

Fig. 11 SEM images of hollow microchannels formed using the EFAC process

polymer. Optimizing the speed of fabrication requires careful control of both voltage and permittivity of the polymer. The study also indicates that the shape of the bottom half of the microstructures can be controlled by altering the initial polymer deposited and the air gap between the polymer and the electrode.

Though there is limited experimental data to validate against the model demonstrates the same behavior as experiments. Here we are looking at the behavior of the process within a parameter space to provide a critical understanding that can be used to inform future experimental work that has already demonstrated feasibility of this process at the laboratory scale. By understanding and then optimizing these parameters the EFAC process be potentially able to be used in high volume manufacturing, significantly reducing the cost of microchannel and enclosed polymer microstructures.

Acknowledgements The authors would like to acknowledge the financial support from the UK Engineering and Physical Research Science Council (EPSRC) through the grants EP/F02553X/1 (Scottish Manufacturing Institute, SMI) and EP/C534212/1 (3D-Mintegration). Financial support from the University of Greenwich is also gratefully acknowledged.

References

Chen H, Yu W, Cargill S, Patel MK, Bailey C, Tonry C, Desmulliez MPY (2012) Self-encapsulated hollow microstructures formed by electric field-assisted capillarity. Microfluid Nanofluid 13(1):75–82

Chou SY, Zhuang L, Guo L (1999) Lithographically induced self-construction of polymer microstructures for resistless patterning. Appl Phys Lett 75:1004–1006

Landau LD, Lifshitz EM (1984) Electrodynamics of continuous media, 2nd edn. Pergamon Press, Oxford

Peeni BA, Lee ML, Hawkins AR, Wooly AT (2006) Sacrificial layer microfluidic device fabrication methods. Electrophoresis 27:4888–4895

Tonry C, Patel MK, Desmuliez MPY, Yu W, Bailey C (2015) Computational electrohydrodynamics in the fabrication of hollow polymer microstructures. In: Thermal, mechanical and multi-physics simulation and experiments in microelectronics and microsystems (EuroSimE), 16th International Conference on

Unger MA, Chou HP, Thorsen T, Scherer A, Quake SR (2000) Monolithic microfabricated valves and pumps by multilayer soft lithography. Science 288:113–116

Wu L, Chou SY (2005) Electrohydrodynamic instability of a thin film of viscoelastic polymer underneath a lithographically manufactured mask. J Nonnewton Fluid Mech 125:91–99

Yue P, Feng JJ, Liu C, Shen J (2004) A diffuse-interface method for simulating two-phase flows of complex fluids. J Fluid Mech 515:293–331